



Atomic-scale heterogeneity in large-plasticity Cu-doped metallic glasses



C.C. Yuan^{a, b, *}, Z.W. Lv^a, C.M. Pang^a, X.L. Wu^b, S. Lan^{b, c}, C.Y. Lu^b, L.G. Wang^b, H.B. Yu^d, J.H. Luan^e, W.W. Zhu^a, G.L. Zhang^a, Q. Liu^b, Xun-Li Wang^b, B.L. Shen^{a, **}

^a School of Materials Science and Engineering, Jiangsu Key Laboratory for Advanced Metallic Materials, Southeast University, Nanjing, 211189, China

^b Department of Physics, City University of Hong Kong, 83 Tat Chee Avenue, Kowloon, Hong Kong, China

^c Herbert Gleiter Institute of Nanoscience, Nanjing University of Science and Technology, Nanjing, 210094, China

^d Wuhan National High Magnetic Field Center, Huazhong University of Science and Technology, Wuhan, 430074, China

^e Center for Advanced Structural Materials, Department of Materials Science and Engineering, City University of Hong Kong, Hong Kong, China

ARTICLE INFO

Article history:

Received 11 March 2019

Received in revised form

13 May 2019

Accepted 24 May 2019

Available online 28 May 2019

Keywords:

Disordered structures

X-ray scattering

Elastic moduli

Deformation and plasticity

Metallic glasses

ABSTRACT

By using nanoindentation techniques combined with transmission electron microscope, wide-/small-angle X-ray scattering, and three-dimensional atom probe tomography, the sub-nanometer- to nanometer-length-scale structural heterogeneity due to the precipitation of Co(Fe)-rich clusters was observed in $[(\text{Co}_{0.7}\text{Fe}_{0.3})_{0.68}\text{B}_{0.219}\text{Si}_{0.051}\text{Nb}_{0.05}]_{100-x}\text{Cu}_x$ ($x = 0.5$) metallic glasses. Such short-range ordered structure promotes energy dissipation during deformation via regulating intrinsic elastic constants and hardness at the mesoscale, which contributes to the improved compressive plasticity of Cu-doped (Fe, Co)-based metallic glasses. Our work provides new evidence on atomic-scale heterogeneity in Cu-doped metallic glasses from the aspects of topological orders and microscopic mechanical responses.

© 2019 Elsevier B.V. All rights reserved.

1. Introduction

Structural heterogeneities widely exist in nature for tailoring the mechanical performance of the material [1–5]. The elasticity, strength, damage tolerance, fracture, and remodeling of ceramics, alloys as well as biological/organic materials such as bone, tooth, mollusk shells, wood composites, etc. can be modulated via varying nano- to micron-scale heterogeneities [1–5].

Recent studies show that the nanoscale heterogeneity is common in metallic glasses (MGs), e.g. two-phase glassy alloys [6], nano-glasses [7], and nano-double-phase glass composites [8], even monolithic MGs [9,10]. It leads to the mechanical heterogeneity at the multiscale [11–13] and effectively enhances the

plasticity of MGs [6,14,15]. As a nanocrystalline producer, Cu element is often doped into Co/Fe-based MGs to stimulate the nucleation of α -(Co, Fe) grains [16,17], owing to a positive mixing enthalpy between Cu and Co/Fe ($\Delta H_{\text{Cu-Co}} = +6 \text{ kJ mol}^{-1}$, $\Delta H_{\text{Cu-Fe}} = +13 \text{ kJ mol}^{-1}$) [18]. This refined α -(Co, Fe) precipitate can improve the soft magnetic performance remarkably [19,20] and simultaneously enhance the mechanical properties of ferromagnetic MGs [16,21,22]. For example, $(\text{Co}_{0.7}\text{Fe}_{0.3})_{0.68}\text{B}_{0.219}\text{Si}_{0.051}\text{Nb}_{0.05}$ MG can barely withstand the plastic deformation, thereby leading to a catastrophic fracture, while the compressive plasticity of $[(\text{Co}_{0.7}\text{Fe}_{0.3})_{0.68}\text{B}_{0.219}\text{Si}_{0.051}\text{Nb}_{0.05}]_{99.5}\text{Cu}_{0.5}$ MG (~2.5%) can be significantly improved upon only 0.5 at.% Cu alloying [22]. However, the convincing experimental evidence for such sub-nanoscale structural features in Cu-doped MGs is missing. The important details such as the characteristic length scale of heterogeneous features, their morphology and spatial distribution, especially their sensitivity on microscopic mechanical responses remain unrevealed.

In order to characterize the atomic-scale structure of Cu-doped MGs, transmission electron microscope (TEM), small-angle X-ray scattering (SAXS), high-energy synchrotron X-ray diffraction, and

* Corresponding author. School of Materials Science and Engineering, Jiangsu Key Laboratory for Advanced Metallic Materials, Southeast University, Nanjing, 211189, China.

** Corresponding author. School of Materials Science and Engineering, Jiangsu Key Laboratory for Advanced Metallic Materials, Southeast University, Nanjing 211189, China

E-mail addresses: yuanchenchenneu@hotmail.com (C.C. Yuan), blshen@seu.edu.cn (B.L. Shen).

three-dimensional atom probe tomography (3D-APT) were conducted in this work. Combined with nanoindentation techniques, the structure and mechanical behaviors of $[(\text{Co}_{0.7}\text{Fe}_{0.3})_{0.68}\text{B}_{0.219}\text{Si}_{0.051}\text{Nb}_{0.05}]_{100-x}\text{Cu}_x$ ($x = 0, 0.5$) MGs at the microscopic scale were investigated in detail via the distribution of nanoscale nuclei, elastic moduli, and hardness.

2. Experimental

Multi-component alloy ingots with nominal compositions $[(\text{Co}_{0.7}\text{Fe}_{0.3})_{0.68}\text{B}_{0.219}\text{Si}_{0.051}\text{Nb}_{0.05}]_{100-x}\text{Cu}_x$ ($x = 0, 0.5$) were prepared by arc melting mixtures of pure Co (99.99 at.%), Fe (99.99 at.%), B (99.999 at.%), Si (99.99 at.%), Nb (99.95 at.%), Cu (99.995 at.%) in a high-purity argon atmosphere. The microstructure of the glassy samples was detected by TEM (Tecnai G2 T20), SAXS using a SAXSpace with Mo $K\alpha$ radiation (Anton Paar, Graz, Austria), and 3D-APT performed in a local electrode atom probe (CAMEACA LEAP 5000 XR). Pair distribution functions of high-energy synchrotron X-ray total diffraction for local structural measurements were carried out at the beamline 11-ID-C, Advanced Photon Source, Argonne National Laboratory. High-energy X-rays with the wavelength of 0.1173 Å were used in transmission geometry for data collection. The nanoindentation tests were conducted using a NanoTest Vantage (Micro Materials Ltd) with a standard Berkovich diamond indenter.

3. Results and discussion

Fig. 1 (a) and (b) show TEM micrographs and the selected area electron diffractions of as-cast non-Cu and Cu-doped $(\text{Co}_{0.7}\text{Fe}_{0.3})_{0.68}\text{B}_{0.219}\text{Si}_{0.051}\text{Nb}_{0.05}$ MGs. For two MGs, the selected area electron diffractions only exhibit several sharp rings. No

obvious diffraction spot is found, indicating a fully amorphous nature. However, at a higher magnification, TEM bright field image of Cu-doped MG apparently shows some ordered nuclei as demonstrated by scattered lattice fringes with diameters less than 3 nm embedded in the amorphous matrix (see left inset in Fig. 1 (b)). According to the selected diffraction patterns of as-cast rod samples with critical diameters in our previous studies [22], these ordered regions are proposed to be the α - (Co, Fe) phase.

Such nanoscale chemical heterogeneity was further proved by SAXS and the resulting $I(Q)$. Fig. 1 (c) illustrates SAXS profiles of non-Cu and Cu-doped MGs. Two curves show a significant increase of intensity at low Q , which is attributed to the scattering from sample imperfections. Interestingly, Cu-doped MG shows a noticeable higher intensity in a broad Q range (from 0.015 to 0.1 \AA^{-1}) in comparison with non-Cu MG. The enhanced scattering in this Q range comes from a larger electron density difference in the range from several to tens of nanometers in real space. It means that Cu-doped MG presents a high degree of heterogeneity. The shape of SAXS profiles shows a broad distribution of characteristic distances for such heterogeneities. The inset in Fig. 1 (c) shows the real space pair distance distribution function $p(r) = (1/2\pi^2) \times \int_0^\infty I(Q)Qr\sin(Qr)dQ$ (PDDF) [23] obtained by the indirect Fourier transformation of $I(Q)$ using GIFT (Anton Paar). Consistent with TEM observation, no sign of phase separations with two distinguishable contrasts as shown by two or multiple characteristic distances is displayed in PDDFs of two MGs [6]. One characteristic distance of heterogeneous regions in both non-Cu and Cu-doped MGs is found to be about 25 nm. Compared with non-Cu MG, the peak value of $p(r)$ for Cu-doped MG is twice higher, further verifying that Cu-doped MG is more inhomogeneous than non-Cu MG.

Fig. 1 (d) shows the total structure factor $S(Q)$ and the reduced pair distribution function (PDF) $G(r)$ obtained by the Fourier

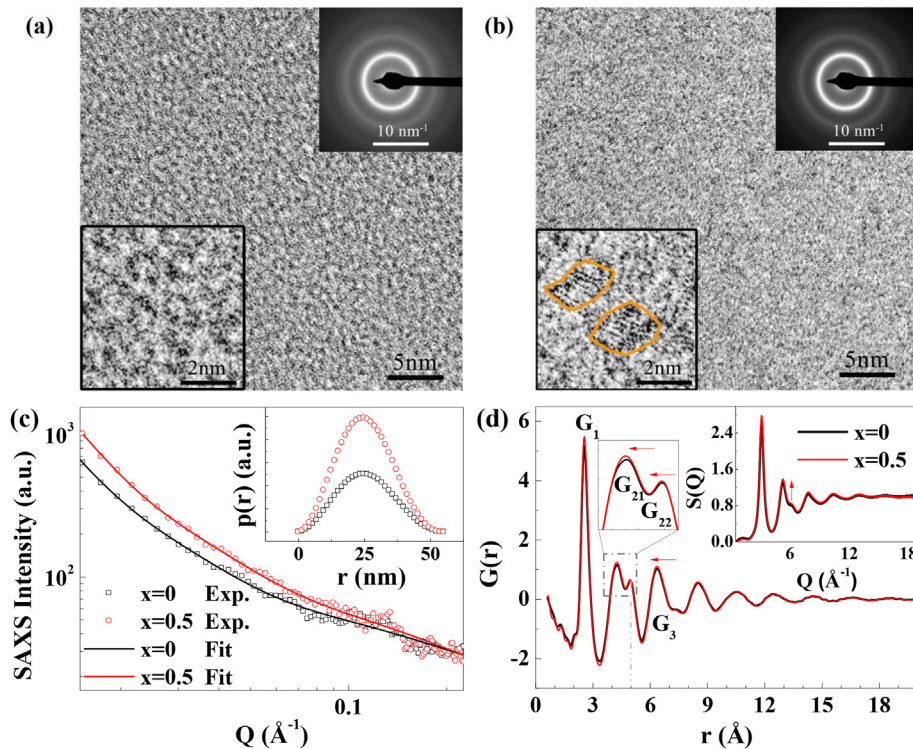


Fig. 1. Microscopic structure of $[(\text{Co}_{0.7}\text{Fe}_{0.3})_{0.68}\text{B}_{0.219}\text{Si}_{0.051}\text{Nb}_{0.05}]_{100-x}\text{Cu}_x$ ($x = 0, 0.5$). TEM bright filed images of MGs: (a) $x = 0$ and (b) $x = 0.5$. The right and left insets in (a) and (b) are the corresponding selected area electron diffraction patterns and the magnification of TEM micrographs, respectively. (c) SAXS results of the as-cast $[(\text{Co}_{0.7}\text{Fe}_{0.3})_{0.68}\text{B}_{0.219}\text{Si}_{0.051}\text{Nb}_{0.05}]_{100-x}\text{Cu}_x$ ($x = 0, 0.5$). The inset in (c) is PDDF obtained from the SAXS results by indirect Fourier transformation. (d) $G(r)$ s from high-energy X-ray diffraction experiment for $x = 0$ and 0.5 respectively. The inset in (d) shows the corresponding $S(q)$ data.

transform of the structure factors. As seen in the inset of Fig. 1 (d), a first sharp diffraction peak of $S(Q)$, followed by a second peak and shoulder characteristics, gives rise to a typical amorphous nature of two MGs. $G(r)$ s present a real-space structure with each peak defined as G_i ($i = 1, 2, 3$, etc.). The short-range order corresponding to the nearest neighbor shell exhibits a sharp first peak G_1 in $G(r)$. A more pronounced short-range order of Cu-doped MG than that of non-Cu MG can be shown by the more intense peak value of G_1 in Fig. 1 (d). A slight shift of peak value of G_2 and G_3 in $G(r)$ towards a lower r with the addition of Cu suggests a denser packing at medium-range orders of 4–7 Å in Cu-doped MG. More interestingly, the intense peak value of G_{21} , G_{22} , G_3 as well as a slightly more obvious shoulder appearing in the second peak of $S(Q)$ with $Q \sim 6 \text{ \AA}^{-1}$, demonstrates a pronounced ordered structure of Cu-doped MG at the length scale of medium-range orders. The obvious short- and medium-range orders of Cu-doped MG well account for the crystalline nuclei found in TEM studies.

Despite the nanoscale heterogeneity observed in both TEM and SAXS, 3D-APT results show no sign of compositional/chemical segregation. Fig. 2 shows the APT analysis of two MGs. The 3D-APT tip reconstruction of all elements in Fig. 2 (a) shows that there is no observable elemental segregation in the investigated volume. Here, the tip of Cu-doped system has an overall composition of $\text{Co}_{43.56}\text{Fe}_{22.71}\text{B}_{20.94}\text{Si}_{6.73}\text{Nb}_{5.59}\text{Cu}_{0.47}$ (at. %), which is quite close to its normal composition of $[(\text{Co}_{0.7}\text{Fe}_{0.3})_{0.68}\text{B}_{0.219}\text{Si}_{0.051}\text{Nb}_{0.05}]_{99.5}\text{Cu}_{0.5}$. One-dimensional concentration profiles of all the elements in Cu-doped MG are also presented in Fig. 2 (b) and (c). It is clear that there is no periodic fluctuation of elemental fractions along the length direction of the tip. A random distribution of all elements can be observed. It seems that the structural heterogeneity as indicated by TEM and SAXS has no contribution from the chemical segregation. Cu doping has a larger impact on topological features of Co(Fe)-based MGs.

Fig. 2 (d) and (e) exhibit the corresponding statistical binomial frequency distribution analysis [24,25]. It can be seen that the binomial curves match the curves obtained from experiments, indicating a totally random distribution with no recognized precipitate. The quality of the fit was quantified using several parameters as listed in the insets of Fig. 2 (d) and (e). Reduced χ^2 is the deviation of the measured distribution from the binomial distribution, which represents the degree of the heterogeneous distribution of sample compositions. $\chi^2 = \sum(N_{\text{obs}} - N_{\text{exp}})^2 / N_{\text{exp}}$, where N_{obs} is the number of bins observed in the experimental data at a certain elemental concentration and N_{exp} the number of bins that expected from a homogenous alloy with random distributions, as modeled by a binomial distribution, n_d the number of degrees of freedom for a given ion, and μ the normalized homogenization parameter. The values of μ for all elements in both non-Cu and Cu-doped MGs are close to 0, confirming the random distribution of all the elements (B, Si, Fe, Co, Nb, and Cu). Reduced χ^2 s for Co, Fe, Nb, Si elements are of the value less than 5, which give rise to an even distribution of all components except for B in two MGs.

The precipitation of the refined α -Co(Fe) phase in the Cu-doped alloy has already been noticed in some studies [16,17,20–22], which is suggested due to the repulsive interaction of Cu with both Co and Fe [18]. It is assumed that Cu-rich clusters as a precursor might form in the glassy matrix before the appearance of α -Co(Fe) nuclei [16,17,22] as a result of a positive mixing enthalpy between Cu and Co(Fe) elements [18]. The Cu-rich clusters have been observed in some other alloy systems as well. For example, Cu-centered icosahedra with fewer Zr and more Cu are found in *ab initio* simulations of $\text{Cu}_{45}\text{Zr}_{45}\text{Ag}_{10}$ combined with the extended X-ray absorption fine structure spectroscopy [26]. It facilitates an atomic-scale chemical heterogeneity, which may lead to strong chemical segregations and even phase separation [26]. However, these atomic-scale

configurations haven't been detected by 3D-APT. In the present work, we find that reduced χ^2 of Cu is close to 0. It experimentally verifies the homogeneous distribution of Cu element in Cu-doped MG. This means that, at the 3D-APT experimental time and length scale, Cu element disperses homogeneously in the glassy matrix rather than segregates together as long as the sample has not been annealed to the partial crystallization [17].

Moreover, the value of reduced χ^2 for B in the Cu-doped MG is twice smaller as compared with that in non-Cu MG. It leaves a hint that the formation of B-rich clusters might be impeded in Cu-doped MG, namely, the addition of Cu restrains the formation of brittle Co(Fe)–B intermetallic phases. This result further confirms that the observed nanoscale ordered structure in TEM intend to be the precursor of α -Co(Fe) phases.

The contour maps in Fig. 3 show the spatial distribution of hardness values and elastic moduli of two MGs over a $210 \times 210 \mu\text{m}^2$ square area. One can see that the islands with high hardness values are surrounded by a continuous zone with low hardness values, resembling to the observation in the large plastic Zr–Cu–Ni–Al MG by the work of Du. et al. [6]. Different from non-Cu MG, the distribution of hardness of Cu-doped MG fluctuates more significantly in the observed size regime. As shown in Fig. 3 (a) and (b), the characteristic sizes of hard regions surrounded by soft regions are about 50–70 and 20–30 μm for Cu-doped and non-Cu MGs, respectively. The area of hard regions in Cu-doped MG is almost twice larger than that of non-Cu MG.

The contour maps in Fig. 3 (c) and (d) show the spatial distribution of elastic moduli values of two MGs. It is found that the average moduli of Cu-doped MG are much higher than that of non-Cu MG, which is attributed to a denser atomic packing at medium-range orders indicated by a shift of peak position of G_2 and G_3 to a low r in PDF patterns [27]. Moreover, in non-Cu MG, the islands with low elastic moduli are surrounded by a continuous zone with high elastic moduli. It is quite different from the distribution of elastic moduli in Cu-doped MG, where the islands with high values of elastic moduli are surrounded by a continuous zone with low elastic moduli, similar to the distribution of hardness. According to TEM [22] and 3D-APT analysis, the soft regions are the precursor of α -Co(Fe) phase made up of Co(Fe)-rich clusters, while the hard regions are the MG matrix. The surrounding high-elastic-moduli Co(Fe)–B regions hinder atomic motion or diffusion during deformation, which leads to poor deformability of non-Cu MGs. While in Cu-doped MGs, a more continuous network structure is formed by weakly-bonded Co(Fe)-rich regions. In virtue of the plastic flows of weakly-bonded regions [14], the stress concentration inside shear bands or at the crack tips is mitigated when a shear band or microcrack contacts with the continuous weakly-bonded regions during its propagation process. It prevents a single primary shear band carrying a large strain or severe deformation locally that induces a catastrophic fracture [28]. This may lead to a large plasticity of Cu-doped MGs [22].

On the other hand, as shown in TEM, SAXS, and high-energy X-ray diffraction, the characteristic size of structural fluctuations induced by Cu is found in the range from several angstroms to dozens of nanometers. It promotes hierarchical heterogeneities at a wide range of characteristic length scales, which leads to the mechanical heterogeneity at the mesoscale [15], as displayed here by the distribution of hardness and elastic moduli in Fig. 3. Besides, such hierarchical heterogeneity also results in the appearance of more bifurcated structure [13], which not only provides more sites for initiating plastic flow at the atomic level (the nucleation of shear transformation zones) but also controls the pathway and the stability of propagation of shear bands, i.e., dissipating more energy during the formation. This further improves the plasticity of Cu-doped MGs.

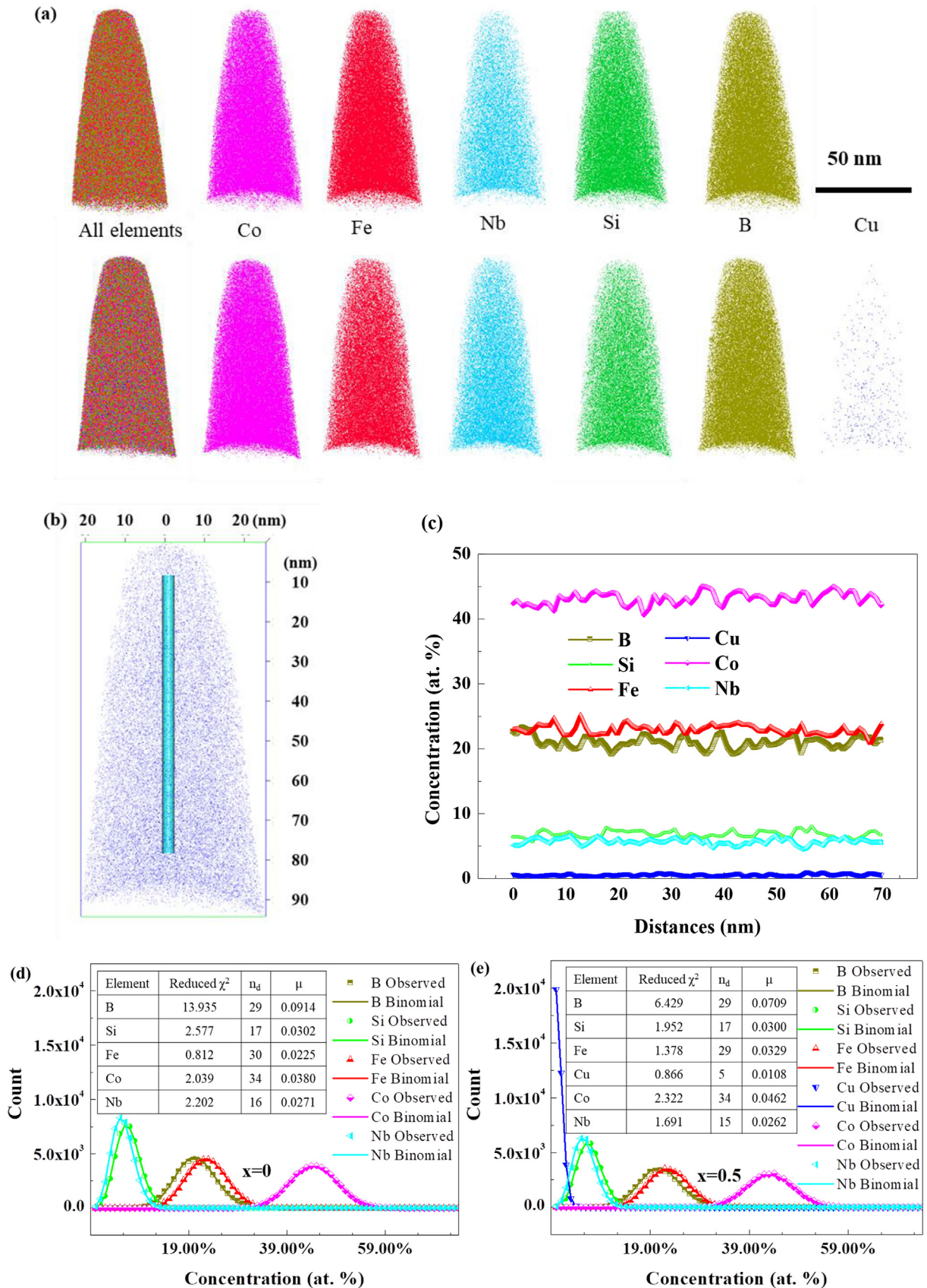


Fig. 2. Representative APT analysis on the as-cast $[(\text{Co}_{0.7}\text{Fe}_{0.3})_{0.68}\text{B}_{0.219}\text{Si}_{0.051}\text{Nb}_{0.05}]_{100-x}\text{Cu}_x$ ($x=0, 0.5$). (a) 3D-APT tip reconstruction of all elements in the samples. (b) The selected regime in 3D-APT tip reconstruction of $[(\text{Co}_{0.7}\text{Fe}_{0.3})_{0.68}\text{B}_{0.219}\text{Si}_{0.051}\text{Nb}_{0.05}]_{99.5}\text{Cu}_{0.5}$ sample along the length direction with the cross section of the diameter of 3 nm. (c) One-dimensional concentration profiles taken along the length direction of the tip shown in (b). Frequency distribution analysis of the composition with $x=0$ (d) and $x=0.5$ (e), obtained both from observed experimental results and from the binomial simulation. Several parameters employed to assess the quality of the fit of the experimental results to the binomial simulation are listed in the inserted table of (d) and (e).

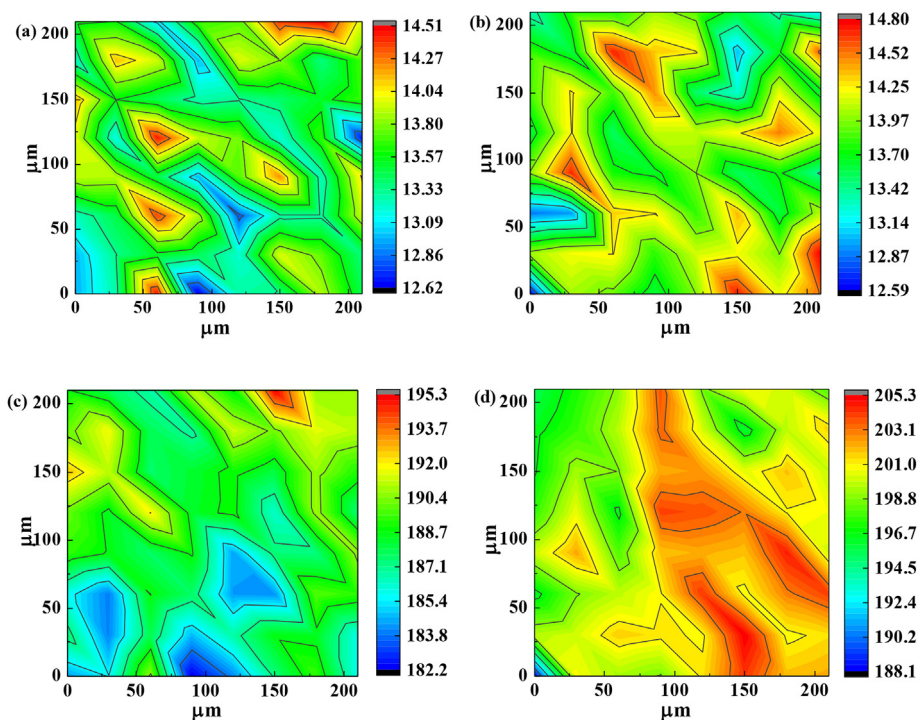


Fig. 3. The spatial distribution of mechanical properties of $[(\text{Co}_{0.7}\text{Fe}_{0.3})_{0.68}\text{B}_{0.219}\text{Si}_{0.051}\text{Nb}_{0.05}]_{100-x}\text{Cu}_x$ ($x = 0, 0.5$). The contour-line maps of the nanoindentation hardness values: (a) $x = 0$ and (b) $x = 0.5$, and of the nanoindentation E : (c) $x = 0$ and (d) $x = 0.5$.

In fact, the mechanical heterogeneity due to the inhomogeneous structure has been reported in many glass composites, owing to the variation of elastic modulus/hardness between the introduced soft crystalline phases and the hard glassy matrix [29–31]. The ductile/soft dendrite phase precipitated in the glassy matrix plays a role similar to that of α -Co (Fe) nuclei/phases in Co(Fe)-based MGs, which can modulate the mechanical properties of MGs by regulating their distribution in the glassy matrix [15,30,32]. It is proposed that the mechanical properties of glass composites can be effectively improved when the dendritic/ductile phase approaches a critical volume fraction and percolates through the sample [30,32]. Also in the case of biomaterials like bone, the extension of an inelastically deformed area, i.e. weakly-bonded region [1] remarkably improves energy dissipation by increasing the micro-mechanical heterogeneity. While in Cu-doped Co(Fe)-based MG, the α -Co (Fe) segregation exhibits a rapid nucleation rate and a sluggish growth rate [17]. It is prone to form a percolated weakly-bonded network in the Cu-doped Co(Fe)-based glassy matrix as shown in Fig. 3 (b) and (d), especially when it is irritated by additional conditions such as annealing [17] or applied loading [29]. The continuous weakly-bonded regions give rise to a high probability of the nucleation of shear transformation zones during the redirection of shear bands/microcracks in a percolated network structure [30,32], which contributes to a preferred plastic deformation rather than brittle fractures in Cu-doped Co(Fe)-based glass composite [16]. On the contrary, the separated soft phases and hard phases formed by the liquid phase separation in Zr-based MG result in relatively lower plasticity [6] as compared with the superplastic Zr-based MG that induced by continuous structural fluctuations [33,34]. Moreover, an atomically sharp crack tip that propagates along a percolating path consisting of a strongly/covalent bonded structure such as nonmetals (B, P, C, etc.)-rich region even leads to the brittle fracture of the material like in Fe–P MG [35]. Our studies on improving the plasticity of Co(Fe)-based MGs by manipulating the mechanical heterogeneity based on the atomic-scale

heterogeneity induced by minor Cu alloying, thus, also can guide the design of Co(Fe)-based or other glass composites with much larger plasticity. Moreover, since nanometer-sized α -Fe precipitates have a composition close to that of the grain-orientated high-silicon steel, the structural design of Co(Fe)-based glass composites at the nanoscale can promote their industrial applications in the field of soft magnetic materials as well [19,20].

4. Conclusions

In conclusion, the structural heterogeneity in the range from sub-nanometer to tens of nanometers in Cu-doped Co(Fe)-based MG was demonstrated by TEM, SAXS, high-energy X-ray diffraction and 3D-APT in this work. It is attributed to atomic-scale topological orders introduced by the positive mixing enthalpy between Cu and Co(Fe). Such structural fluctuations induce a mechanical heterogeneity at the micron scale. Our studies show that a pronounced hierarchical heterogeneity and the continuous weakly-bonded soft regions in Cu-doped MGs facilitate more energy dissipation during deformation, which may provide a possible underlying mechanism for understanding the improved plasticity in Cu-doped MGs/glass composites as well as other composite materials in nature.

Acknowledgments

This work was supported by the National Natural Science Foundation of China (Grant Nos. 51601038 and 51631003), the Natural Science Foundation of Jiangsu Province, China (Grant No. BK20171354), Postdoctoral Fellow under the Hong Kong Scholar Scheme (Grant No. XJ2017048), Jiangsu Key Laboratory for Advanced Metallic Materials (Grant No. BM2007204). High energy X-ray diffraction was conducted at the Advanced Photon Source, a U.S. Department of Energy (DOE) Office of Science User Facility operated for the DOE Office of Science by Argonne National Laboratory under Contract No. DE-AC02-06CH11357. Atom probe

tomography research was conducted at the Inter-University 3D Atom Probe Tomography Unit of City University of Hong Kong supported by the CityU grant 9360161.

References

- [1] K. Tai, M. Dao, S. Suresh, A. Palazoglu, C. Ortiz, *Nat. Mater.* 6 (2007) 454–462.
- [2] E. Ma, T. Zhu, *Mater. Today* 20 (2017) 323–331.
- [3] D.C. Stahl, S.M. Cramer, R.L. Geimer, *Wood Fiber Sci.* 29 (1997) 345–352.
- [4] G.A. Song, J.H. Han, T.E. Kim, J.M. Park, D.H. Kim, S. Yi, Y. Seo, N.S. Lee, K.B. Kim, *Intermetallics* 19 (2011) 536–540.
- [5] K. Bhattacharya, M. Ortiz, G. Ravichandran, *J. Mech. Phys. Solids* 46 (1998) 2171–2181.
- [6] X.H. Du, J.C. Huang, K.C. Hsieh, Y.H. Lai, H.M. Chen, J.S.C. Jang, P.K. Liaw, *Appl. Phys. Lett.* 91 (2007) 131901.
- [7] H. Gleiter, *Small* 12 (2016) 2225–2233.
- [8] G. Wu, K.-C. Chan, L. Zhu, L. Sun, J. Lu, *Nature* 545 (2017) 80.
- [9] J. Ding, S. Patinet, M.L. Falk, Y. Cheng, E. Ma, *Proc. Natl. Acad. Sci. Unit. States Am.* 111 (2014) 14052–14056.
- [10] F. Zhu, S.X. Song, K.M. Reddy, A. Hirata, M.W. Chen, *Nat. Commun.* 9 (2018) 11–20.
- [11] Y.H. Liu, D. Wang, K. Nakajima, W. Zhang, A. Hirata, T. Nishi, A. Inoue, M.W. Chen, *Phys. Rev. Lett.* 106 (2011) 125504.
- [12] H. Wagner, D. Bedorf, S. Küchemann, M. Schwabe, B. Zhang, W. Arnold, K. Samwer, *Nat. Mater.* 10 (2011) 439–442.
- [13] P. Tsai, K. Kranjc, K.M. Flores, *Acta Mater.* 139 (2017) 11–20.
- [14] E. Ma, J. Ding, *Mater. Today* 19 (2016) 568–579.
- [15] B. Sarac, Y.P. Ivanov, A. Chuvilin, T. Schoberl, M. Stoica, Z.L. Zhang, J. Eckert, *Nat. Commun.* 9 (2018) 1333.
- [16] X. Li, H. Kato, K. Yubuta, A. Makino, A. Inoue, *Mater. Sci. Eng. A* 527 (2010) 2598–2602.
- [17] Y. Wu, H.X. Li, J.E. Gao, H. Wang, X.J. Liu, M.K. Miller, H. Bei, Y.F. Gao, Z.P. Lu, *J. Alloy. Comp.* 688 (2016) 822–827.
- [18] A. Takeuchi, A. Inoue, *Mater. Trans.* 46 (2005) 2817–2829.
- [19] Z.Z. Li, A. Wang, C.T. Chang, Y.G. Wang, B.S. Dong, *Intermetallics* 54 (2014) 225–231.
- [20] F.L. Kong, H. Men, M.X. Zhang, T.C. Liu, G.Q. Xie, B.L. Shen, *Appl. Phys. A* 108 (2012) 211–215.
- [21] B. Shen, H. Men, A. Inoue, *Appl. Phys. Lett.* 89 (2006) 101915.
- [22] G.L. Zhang, Q.Q. Wang, C.C. Yuan, W.M. Yang, J. Zhou, L. Xue, F. Hu, B.A. Sun, B.L. Shen, *J. Alloy. Comp.* 737 (2018) 815–820.
- [23] A. Guinier, G. Fournet, John Wiley, New York, 1955.
- [24] Z. Li, F. Kormann, B. Grabowski, J. Neugebauer, D. Raabe, *Acta Mater.* 136 (2017) 262–270.
- [25] J.Y. Shin, S. Yi, K.G. Pradeep, P.P. Choi, D. Raabe, *Kor. J. Mater. Res.* 23 (2013) 190–193.
- [26] T. Fujita, K. Konno, W. Zhang, V. Kumar, M. Matsuura, A. Inoue, T. Sakurai, M.W. Chen, *Phys. Rev. Lett.* 103 (7) (2009), 075502.
- [27] D. Ma, A.D. Stoica, X.L. Wang, Z.P. Lu, B. Clausen, D.W. Brown, *Phys. Rev. Lett.* 108 (2012), 085501.
- [28] T.C. Huftnagel, C.A. Schuh, M.L. Falk, *Acta Mater.* 109 (2016) 375–393.
- [29] C.C. Hays, C.P. Kim, W.L. Johnson, *Phys. Rev. Lett.* 84 (2000) 2901–2904.
- [30] M.L. Lee, Y. Li, C.A. Schuh, *Acta Mater.* 52 (2004) 4121–4131.
- [31] S. Pauly, S. Gorantla, G. Wang, U. Kuehn, J. Eckert, *Nat. Mater.* 9 (2010) 473–477.
- [32] J. Kim, H.S. Oh, W. Kim, P.P. Choi, D. Raabe, E.S. Park, *Acta Mater.* 140 (2017) 116–129.
- [33] Y.H. Liu, G. Wang, R.J. Wang, D.Q. Zhao, M.X. Pan, W.H. Wang, *Science* 315 (2007) 1385–1388.
- [34] J.G. Wang, D.Q. Zhao, M.X. Pan, C.H. Shek, W.H. Wang, *Appl. Phys. Lett.* 94 (2009), 031904.
- [35] Y.Z. He, P. Yi, M.L. Falk, *Phys. Rev. Lett.* 122 (2019), 035501.